Calibration of Bi-prism Stereo Systems: A Model Free Approach

Supun Dissanayaka[1,*], Pitikhate Sooraksa[1], Somyot Kaitwanidvilai[2] and John Morris[3]

[1]Robotics and AI, School of Engineering, King Mongkut's Institute of Technology Ladkrabang, Latkrabang, Latkrabang, Bangkok, 10520, Thailand

[2]Electrical Engineering, School of Engineering, King Mongkut's Institute of Technology Ladkrabang, Latkrabang, Latkrabang, Bangkok, 10520, Thailand

[3]School of Industrial Education and Technology, King Mongkut's Institute of Technology, Ladkrabang, Latkrabang, Latkrabang, Bangkok, 10520, Thailand

***Corresponding Author E-mail:** supun.di@kmitl.ac.th

Received: Mar 14, 2024; **Revised:** Jun 24, 2024; **Accepted:** Jun 26, 2024

Abstract

A simple stereo system can be constructed from a single camera using a prism in the optical path to provide the required two views of a system. The simplicity of these systems has several advantages, particularly if the target is an underwater robot, where compact size and ability to seal the optical components are key factors. However, dispersion by the prism, in addition to the lens distortion, makes calibration challenging. By using a model-free approach, we were able to calibrate a prism-based stereo system effectively. We also aimed to use readily available 45° prisms, which present significant dispersion in the system, but retain simplicity and reduce cost, compared to custom low angle prisms. Modern LEDs provide high intensity, low bandwidth light sources and we used a set of three sources, roughly centered on the RGB channels of a readily available commercial camera. Our system used a circular target pattern covering the binocularly visible region in the scene and collected sets of images at known distances, using three separate light sources. From these images, we generated two look-up tables, one for each pixel in the image and a disparity derived by matching corresponding points, $\mathcal{C}$p(u,v,du), which has three dimensions, and another look-up table, which has a single dimension, $\mathcal{C}$z(z), so are not quite large, and not beyond the memory capability of even small modern camera systems, but provide fast, $\mathcal{O}$(1), lookup times, suitable for real-time systems. Our calibration strategy enables a simple stereo system built from a single camera to measure depths in a scene: the single camera requires no electronic synchronization and is built from a single, inexpensive, and readily available optical component – a right-angle prism.

Keywords: Bi-prism, Stereo, Calibration, Monochromatic

1. Introduction

Conventional stereo vision systems refer to **Figure 1(a)** are commonly used in 3D depth measuring applications, for example autonomous driving, mobile robot navigation, automated defect identification, medical applications, industrial inspection systems to monitor products to maintain quality and consistency in production, etc. Physical qualities, e.g. length, height, diameter, surface roughness and complex shape measurement, are being replaced by non-contact stereo visions, as contact less, non-destructive measurements, do not damage or waste material.

In autonomous driving and robot navigation, stereo vision needs high resolution images, without requiring moving parts or energy emission, unlike laser scanners, acoustic or radar sensors

[1],[2]. Usually, camera pairs capture two views of a scene with two cameras, but this requires accurate camera synchronization, and several external and internal parameters, including accurate location and alignment of the cameras and correction for optical aberrations. Thus, significant hardware and the needed space, adds significant cost to gain advantages over other vision systems [3]. Therefore, a single camera stereo refers to **Figure 1(b)** vision may be less expensive, more compact, and simpler to implement. However, as with all stereo vision systems, calibration is crucial to achieve accurate 3D depths. Here, we describe a successful calibration of an inexpensive and simple system, consisting of a single camera and an inexpensive, readily available right-angle prism.

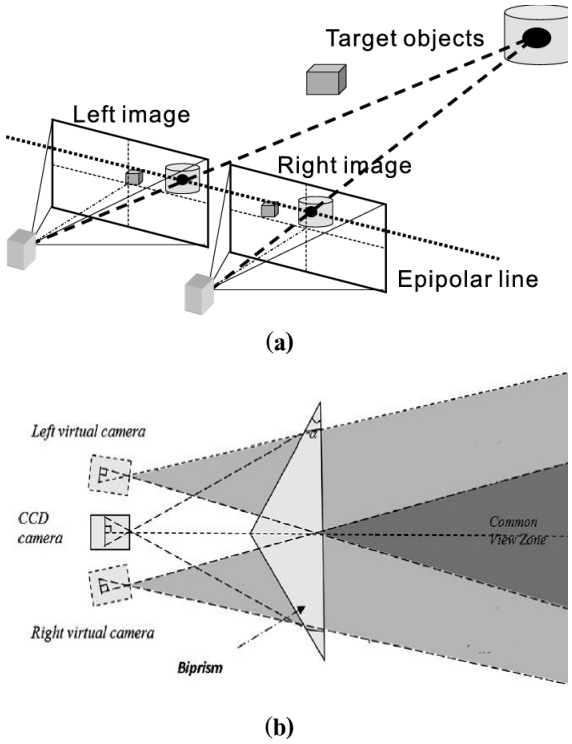

Figure 1 Stereo vision systems (**a**) Conventional stereo vision system representation (**b**) Single camera bi-prism stereo vision system approach

2. Related Work

Rapidity, robustness, and accuracy are the major challenges faced by camera calibration algorithms. Camera calibration generally uses both linear and non-linear techniques. Linear models use a pinhole camera model to find parameters, by solving sets of equations describing image, camera, and world coordinate systems. These models compute rapidly, but accuracy suffers if real lens distortion is neglected [4]. Non-linear models consider lens imperfections and distortions to improve accuracy [5],[6]. Zhang placed a planar pattern in front of a camera, in more than two different orientations to obtain a robust calibration, followed by a set of linear equations to find the camera parameters. Also, he used a non-linear approach to model the radial distortion of the lens [7]. Zhang also tested a camera calibration method using a 2.5D coding target, which required a single captured image capable of calibrating all camera parameters, including a distortion model [8]. The majority of these calibrations were applied to two camera stereo vision systems.

2.1 Two camera stereo calibration

Accurate calibration of two camera stereo systems depends critically on several factors. Systems must be rigid since the relative orientation and separation of the two cameras must stay constant. Also, it is essential to capture the scene with two (or more) cameras simultaneously. Matching features in both images is the stereo correspondence problem - it includes having a 'binocular field of view' (a field in which matching features in both images may be seen), as well as ensuring, as much as possible, identical conditions to simplify feature matching. Movement of the object will cause this matching of individual scene points to be harder. Varying illumination also causes the intensity of individual scene points to vary and not match accurately: synchronization ensures that individual 'shots' of the scene use the same illumination. Thus, identical image conditions, allowing only the view to vary, are needed to detect the matching features, in both left and right images, in the binocular region refers to **Figure 1(b)**, from which depths can be calculated [9].

2.2 Single camera stereo systems

Our system eliminated part of the hardware problem, by using a single camera, equipped with a bi-prism so that images are captured synchronously, 'freeze' motion to the limit allowed by the aperture time, use identical lighting, a single, common lens and identical electronic gain settings. However, the bi-prism introduced an extra distortion, added to the lens distortion, which must be eliminated and much of this paper discusses reducing the prism distortion.

2.3 Previous single camera systems

Several single camera techniques have been described, which ensure synchronization but add complex optical hardware, e.g. multiple mirrors to generate two separate 'views' of the scene. Mouaddib et al. used several convex mirrors to generate these views [10]. Takahashi et al. also used mirrors to observe known points of an object in three poses to calibrate the extrinsic parameters [11]. Another single camera stereo vision used polarizers and mirrors to generate two optical paths and two views [12].

These systems require complex installations, with multiple mirrors or additional polarizers and special mirrors. Polarization led to a significant loss of light, creating a problem in image matching and subsequent calibration difficulties.

2.4 Bi-prism systems

Introducing a bi-prism with a single camera reduced the hardware complexity. Lee and Kwoen used a bi-prism that captured a stereo image pair, due to differing refraction through two sections of a prism - using an arrangement similar to that shown in **Figure 1(b)** [13]. Lim and Xiao similarly placed a bi-prism in the optical path to find the extrinsic parameters of the virtual cameras thus created [3]. Genovese *et al.* noted that distortion induced by the bi-prism could not be handled by existing lens distortion correction functions and chose a model-free approach by calculating a 'piece wise' function, that described the image deformation over the measured area [14].

For a successful configuration, the apex of the prism should divide the field of view (FOV) in half, thus creating two virtual cameras. Pan *et al.* placed a high quality telecentric lens in line with a semi bi-prism to ensure sharp captured images. The distance between lens and prism was manually adjusted, to generate two images from virtual cameras, on the camera sensor. Further, Pan et al. used a monochromatic (blue) light source to avoid prism dispersion problems. Attaching a bandpass filter to the lens helped to eliminate the effects from chromatic aberration included by the prism [15],[16]. Since these methods are needed special setups, e.g. a custom fabricated bi-prism, monochromatic light, or bandpass filters and a telecentric lens, we explored the possibility of achieving similar results, using readily available prisms and a simple camera setup. Using readily available and inexpensive lenses, cameras, and prisms, and thus some not precisely known configuration parameters, e.g. position of the prism relative to the system optical center, we were able to introduce a simple prism distortion correction method, followed conventional lens distortion removal in the camera calibration procedure.

3. Methods

This section describes the simple economic system we created. Camera and prism properties are described in **Table 1.**

Geometric setup

A mount for the prism, in front of the camera lens, to which the camera PCB could be bolted, was 3D printed - see **Figure 2** - in front of the camera lens. The base of the prism was placed as close as possible to the camera lens. The prism apex was roughly aligned with the optical axis of the camera, so that the bi-prism divided the camera sensor in half. Note that the prism exchanges the sides of the captured scene image:

Table 1 Camera and prism properties

Parameter	Value	Note
Camera	Raspberry Pi camera V2	
Sensor Resolution	3280 × 2464 pixels	8 Megapixels
Pixel Size	1.12μ × 1.12μ	Sony IMX219
FOV	62.2°	Horizontal
Focus	1m to infinity	Fixed focus
Light Source	RGB	
Prism		
Material	N-BK7	Right angle prism
Refractive index	1.515	
Angle	45°	
Length of legs	15 mm	
Surface flatness	λ/8	

A multicolor strip of LEDs, with red, green, and blue LEDs, was mounted on a large board. The prism and camera were inserted into an aperture in this board - see **Figure 3**. No alignment in this system was particularly critical, although as noted in the conclusion, the overall calibration curves would be smoother if the prism was better aligned with the camera. The target was imaged, alternately with each color.

A diagram of the setup is in **Figure 4.** The left half shows the transit of a ray through the prism, labelling angles relative to the edges of the prism. The right half shows - viewed from the top and from left to right - the camera image plane, the lens, the prism and three points in the scene. **X**q is a scene point, imaged onto two points - following two paths through the prism, $\mathbf{P}_L$ and $\mathbf{P}_R$, on the image plane. A point, $\mathbf{X}_L$, in the lower half of the scene, is imaged to $\mathbf{P}_L$, which is on the left side of the image points, i.e. the images are reversed. Thus, we have two virtual cameras, viewing a 'binocular region', similar to the conventional stereo vision in **Figure 1(b)**, required for 3D depth calculation.

3.1 Design calculations

To calculate the depth of a scene object, we must have two views of it from different viewpoints (or virtual viewpoints in a bi-prism system). Thus, a key step in designing the system is calculating the binocular region, in which scene points are seen by both cameras (or virtual cameras in our system, since the prism makes it appear as if there are two separate cameras). We back projected rays from the image plane to the scene point: **Figure 4(b)**, shows the bi-prism stereo vision system and an associated co-ordinate system. The points, (**X, Y, Z**), represent a scene point $\mathbf{X}_q$, whereas (u, v) represents image coordinates. The prism angle was α, d is the distance from the optical center, **C**, to the bi-prism and f is the focal length and δ is the deviation of a ray as it passed through the prism.

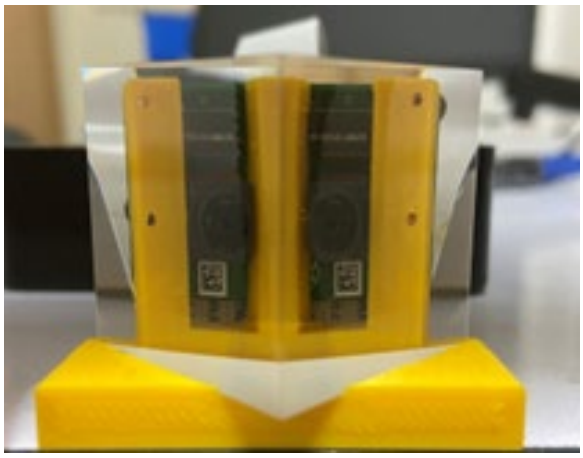

Figure 2 Prism - camera mount

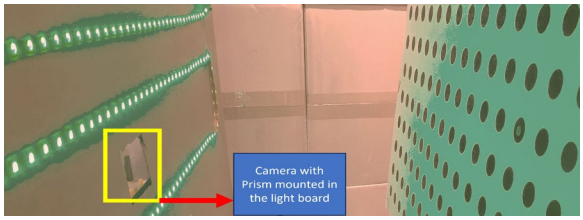

Figure 3 Light board with stereo rig inserted in center

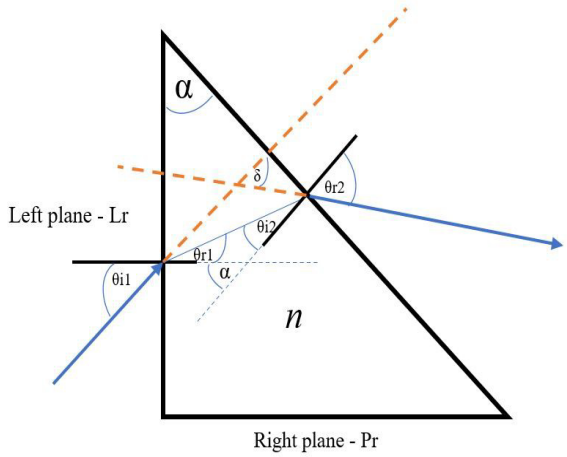

(a)

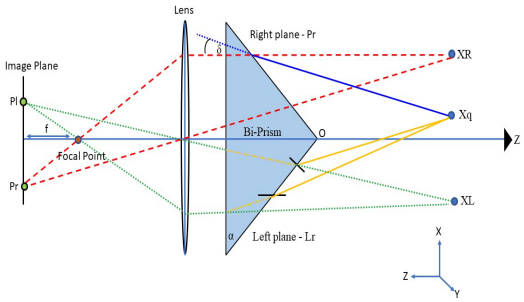

(b)

Figure 4 (**a**) Above shows a model for an incident ray from the left, transiting the prism and exit refracted ray. on the right, on the right, the actual scene point, X_q, is marked and the two 'virtual points', X_L and X_R, generated by the presence of the prism are shown. (**b**) Below are shown as P_L and P_R, the points on the image plane matching X_L and X_R. Model of whole bi-prism vision system.

Back projection simplified the calculations [17]. From the left of **Figure 4 (a)**, we obtain in Equation (1)

$$\alpha = \theta_{r1} + \theta_{i2} \quad (1)$$

where θ_{ix} and θ_{rx} are the incident and refracted angles at surface, $x \in \{1, 2\}$. The total deviation of a back projection ray from the image plane, with incident angle, i1, on the 'front' (base) surface of the prism, is

$$\delta = \theta_{i1} + \theta_{r2} - \alpha \quad (2)$$

3.1.1 Binocular region

To determine the binocular region, we first consider the rays parallel to the optical axis. Note that if the prism angle α is larger than the critical angle, $\theta c = \sin^{-1}(n_1/n_2)$, there will be a small angular field, close to the optical axis, in which rays are totally internally reflected. For a 45° BK-7 prism, $\theta c = \sin^{-1}(1/1.5) = 41.8°$, from BK-7 to air, so that a narrow angular field of 3.2°, between **OE** and **OF**, does not appear in images. The largest emitted angle comes from rays emitted at grazing incidence to the prism edge, i.e. at α = 45° from the optical axis, rays **AB** and **AD**, marked in yellow in **Figure 5.** The other edges of the binocular region are determined by the field of view of the camera: examples are the rays **BC** and **DC**. Note that there is a point, **C**, at which the disparity is zero, as usual for a verging axis stereo camera system. The resulting binocular region is labelled in **Figure 6 and 7**.

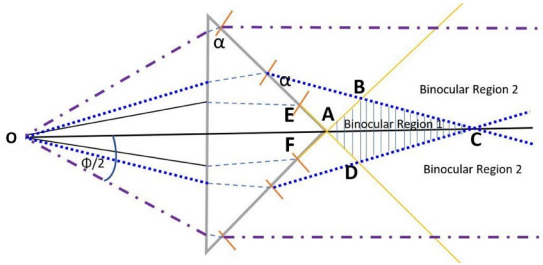

Figure 5 Definition of the binocular region: the 'world' scene region in which depths can be inferred.

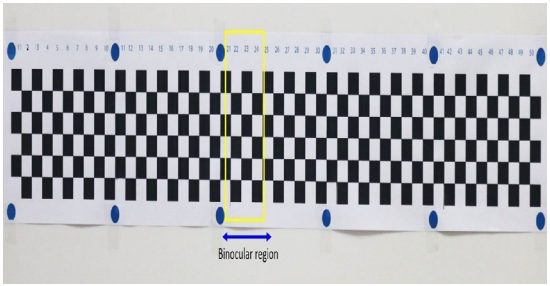

Figure 6 Wide target seen without the prism in the path

Note that the binocular region marked here is a relatively narrow region of the field of view. The yellow boxes outline regions which appear in both images.

Figure 7 Wide target used to illustrate scene setup and prism distortion.

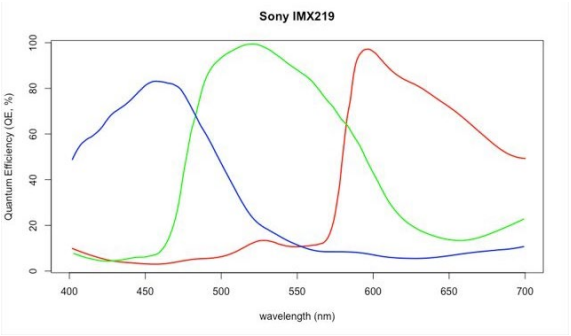

Figure 8 Spectral response of the Sony IMX219 chip

After passing through the prism, rays are deviated by δ, see Equation (2). So, the other edge of the binocular region is determined by the extreme rays in the camera field of view. Two examples are shown in **Figure 5**, for a narrow lens (inner pair of dotted blue rays) and a wider lens (outer pair of dot-dash purple rays). After transiting the prism, rays from the wider lens extend to ∞ and define the binocular region labeled 'Region 2'. Rays from the narrow lens intersect at **C** and delimit the striped binocular region. Thus, designers can choose a lens that leads to a needed binocular region, i.e. areas of interest in which depths can be measured.

A further example appears in the test pattern in **Figure 6**, where the binocular region, shown by numbered columns, which appear in both left and right images, are marked in the lower image.

3.2 Dispersion

Introducing a prism into the optical path of a camera ensures that color images will 'spread' due to the variation of the refractive index, and rays of different colors will diverge as they pass through the prism. Thus, if we wish to image colored scenes, we must allow for these divergences. Several previous studies [15],[18],[19] avoided this problem by using monochromatic light sources or filters. However, if we wish to compute depths in arbitrary scenes, where we cannot control the imaging wavelength or objects in the scene (see **Figure 8**) that might have, conveniently, narrow bands of colors, that assist image matching, we must make allowances for these divergences.

3.3 Calibration of a general bi-prism system

In this section, we describe the calibration model and the challenges in calibrating our bi-prism system. It describes some design trials, not all successful, but reported here for the benefit of following researchers, and the final scheme used to calibrate our system. It discusses the targets, their shapes, and colors.

3.3.1 Camera Calibration Procedure

The basic calibration steps follow traditional patterns using known targets, e.g. checkerboards or patterns of circles, that cover the useful region in the scene, so that optical aberrations can be removed and simple projective geometry based on pinhole camera models used for depth estimation, e.g. Lee and Kweon [13]. However, prism generated aberrations need to be removed first. These aberrations can be seen in **Figure 9**, where it is notable that, even though the target was held perpendicular to the optical axis, so that all squares would appear with similar widths, as seen in the **Figure 7**, with the prism removed. In the lower image, although the squares have similar widths over a small region, e.g. the binocular region marked, significant variations remained. However, this variation was close enough to linear to avoid complex inverse tan corrections, and a need to know the actual angle at which any square corner appears. Thus, we employed Eq. (2) to calculate the total deviation, which allowed us to back-project the rays and determine the position of each scene point on the image plane.

However, this approach has limitations due to the edge distortion induced by lens and chromatic aberration.

Therefore the OpenCV corner detector was not able to detect the distorted edges.

3.3.2 Checkerboard target

The traditional black and white checkerboard used by Zhang [7] (see the **Figure 7**) was rejected for several reasons:

Figure 9 Chromatic aberration induced by prism

- Dispersion also caused significant chromatic aberration.
- Consequently, the 'corners' were not precise and the Harris corner detector often failed to find them.
- With white light source, the vertical edges were dispersed over many pixels, although the horizontal edges (perpendicular to the prism apex) were relatively unaffected - see **Figure 9.**

3.3.3 Circle target approach

Circular patterns have also been used by many - who believed that detecting circle centers was easier, for example, Hui et al. used a solid circle pattern with different diameters to calibrate their stereo vision system [20]. Simple trials with colored circles on a white background in white light - see **Figure 10**, assuming that the R, G, B channels of the camera would select monochromatic images, but the fuzzy images resulted from the white background - see **Figures 11–13**. Fundamentally, all trials with various color combinations and shapes of targets were defeated when using white light imaging sources with the prism in place. Selecting color bands using the inherent filters of the camera or choosing targets with narrow bands of color failed to produce desired sharp images needed for accurate calibration: either the target edges were blurred or, equivalently, the colored background edges were blurred. The use of multiple bi-colored targets was rejected as being impractical due to the number of targets needed and the difficulty of finding suitable colors with minimal spectral overlaps in the camera spectral responses.

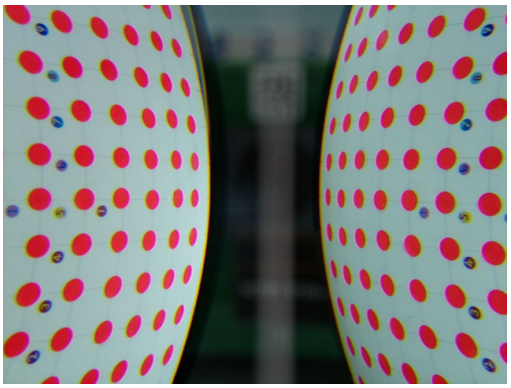

Figure 10 Red circles under white light

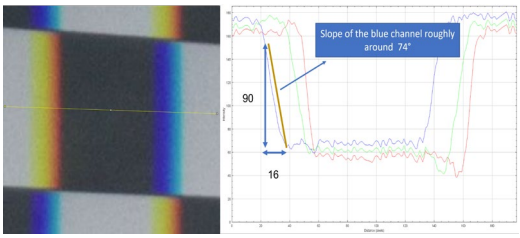

Figure 11 Square target vertical edge distortion; showing in the right panel plots of intensities in the separate RGB channels

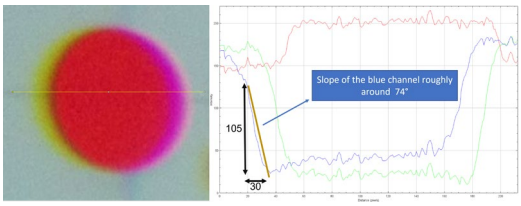

Figure 12 Colored circle target contour distortion

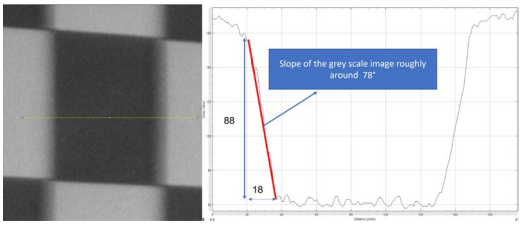

Figure 13 Visible edge dispersion of the target image in grayscale

3.4 Monochromatic illumination

The ready availability of strips of LED lights of various colors prompted a trial using monochromatic illumination. We tested a black and white circle target under monochromatic light see **Figure 14**. Black circles on a white background were selected for our work, over red circles on a white background since red circles did not appear in red channel. Selected target printed onto a 2 × 1 m white plastic background. One dot was chosen as the 'reference' and marked with a white circle in its center see **Figure 14**. While not critical, it made it easy to recognize corresponding points in the left and right images when the prism was inserted into the optical path.

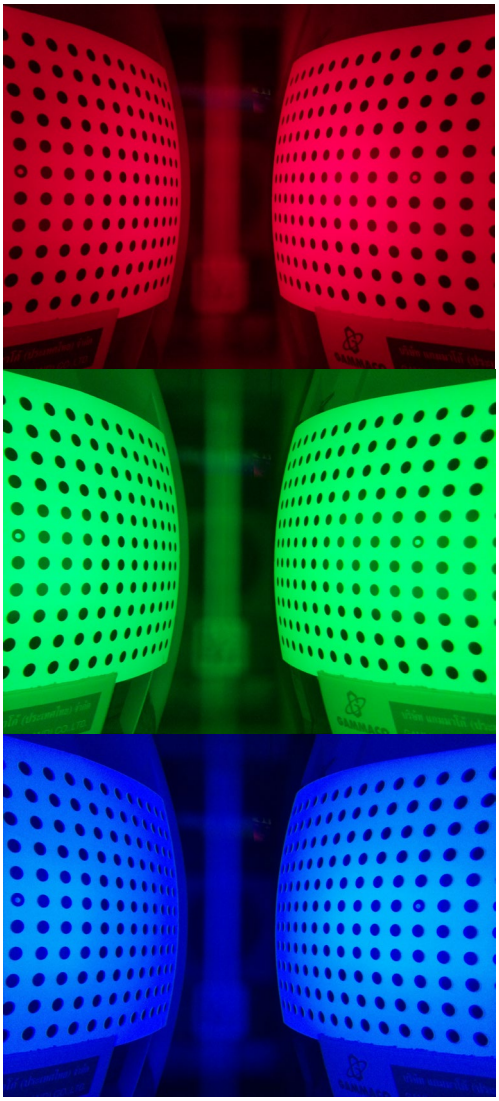

Figure 14 Circle features under red, green, blue illumination

Circle target under monochromatic illumination shows clear circle contour shapes considerably similar to the calibration target under white light without the prism - see **Figures 15–16**.

3.5 Calibration steps

Several images were captured for each illumination (Red, Green, Blue) at each target distance (z = 600, 700, ..., 1200 mm). Processing steps:

1. Images at depths from z = 600 mm to z = 1200 mm were individually processed.
2. Regions of interest (ROIs) were selected.
3. RGB images were separated into color bands: only the color band corresponding to the illumination was used.
4. Images were inverted and thresholded to form binary images.
5. The centers of the images were estimated manually and by our program.
6. Images were separated into left and right regions relative to the center.
7. Targets were identified in the left and right half images- see **Figure 17**.
8. Targets were linked into a rectangular grid- horizontally and vertically - see **Figure18**.
9. Grid points were assigned indices to label corresponding targets in left and right halves - see **Figure19**.
10. and matching disparities, (du), $\mathcal{C}$p(u,v,du), and sets of distances, Cz(z).

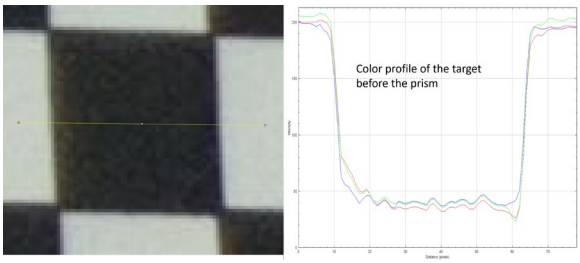

Figure 15 Target image square, a single channel taken from RGB image without the prism

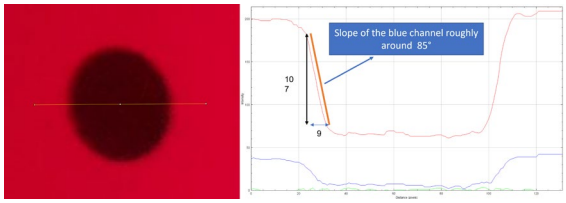

Figure 16 Circle target under red light with prism in the optical path: note the sharper image – higher slope of intensity vs distance in right panel.

3.5.1 Creation of depth maps

Using the two look-up tables, $\mathcal{C}$p, containing (u,v,d) points and the corresponding look-up table, $\mathcal{C}$z of distances, z, to create a depth map for a new, unknown image, $\mathcal{J}$, the steps are:

1. Using the two look-up tables, $\mathcal{C}$p, containing u,v,d points and the corresponding look-up table, $\mathcal{C}$z of distances, z.
2. Identify left and right images, $\mathcal{J} \longrightarrow (\mathcal{J}_L, \mathcal{J}_R)$.
3. Form a depth map large enough to encompass the binocular region in the left image, $\mathcal{J}_L$,
4. For each recognizable point in the left image at u_L,v_L, using any of the several available matching strategies, e.g. SDPS [21], find the corresponding point (u_R,v_R) in the right image.
5. Calculate the disparity, d from the (u_L,v_L)$\longrightarrow$(u_R,v_R) vector.
6. Locate the 8 points surrounding the point (u_L,v_L,d) in the point look-up table, $\mathcal{C}$p.
7. Using the offsets from the points in $\mathcal{C}$p computed by linear interpolation, compute the required z, again by linear interpolation from points in the $\mathcal{C}_z$ table.
8. These z's form the (sparse) depth map.

The sparsity of the depth map will depend on the original image, the number of recognizable matching points in it and the matching algorithm, i.e. how dense are the matching points.

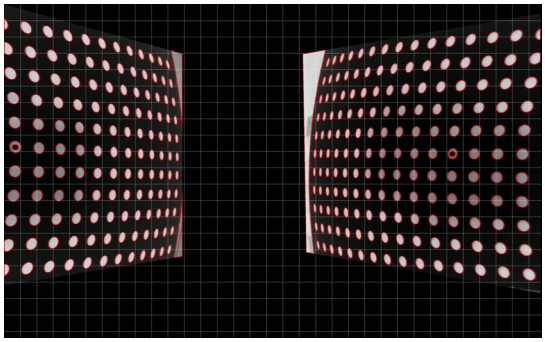

Figure 17 Contours detected after inversion, thresholding and binarization. Note: (1) Large contours resulting from the target board edges were rejected by size, (2) Small targets inside centers of a large target were used to mark corresponding left and right targets - detected as 'inside' larger targets and rejected in the next step

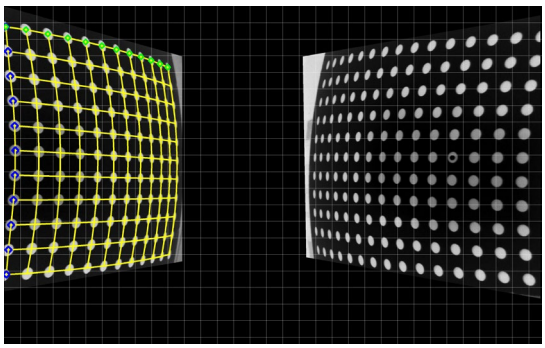

Figure 18 Left Image: Individual target circles linked to rectangular grid

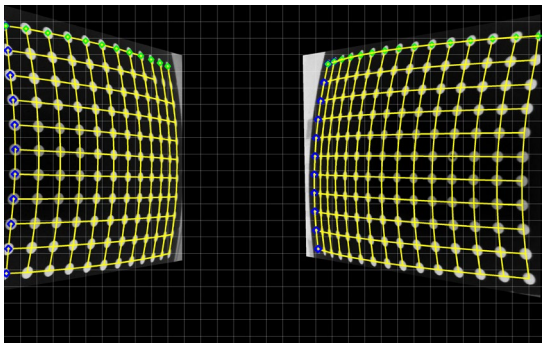

Figure 19 Left and Right: Individual target circles linked to rectangular grid to match the corresponding points

3.6 Pseudocode

A more formal discussion of the several steps in the calibration follows as pseudocode.

Calibration

for each z ∈ (600,700, ... ,1200) do

for each band ∈ (red, green, blue) do

findCorrespondences() (Alg 2)

end

end

Algorithm 1: Overall process

findCorrespondences()

Data: image list (I_j ∈ 0..n − 1)

Result: Calibration map

for each I_j in image_list **do**

A ⟵I^c_j Select c ∈ R, G, B channel from RGB image

B ⟵A Working image - Choose region interest:

mask out background

C ⟵B Invert image

D ⟵C Threshold image

locateCircleCentres()

irj ⟵ Rotate ij using corresponding points;

end

Algorithm 2: Calibration Steps

3.7 Results

We used a stereo vision method, that was able to find the depth of a scene point, z, using two look-up tables. The observable range of depth varies from 600 - 1200 mm due to the limitation of the camera and the prism parameters - see **Table 1**. The first look-up table was produced using the image pixel space Cp, it is sparse and has elements (u, v, du). The second look-up table has the known distances, z, in $\mathcal{C}$z, matching elements in $\mathcal{C}$p. Examples of curves showing elements in $\mathcal{C}$p appear in **Figure 20**, which show that smooth curves for disparity versus distances were extracted from the images for known individual distances. To improve the accuracy of the detection of (u, v) target points, we were able to make three calibration curves - one for each RGB color band, so that **Figure 20** shows sets of three curves.

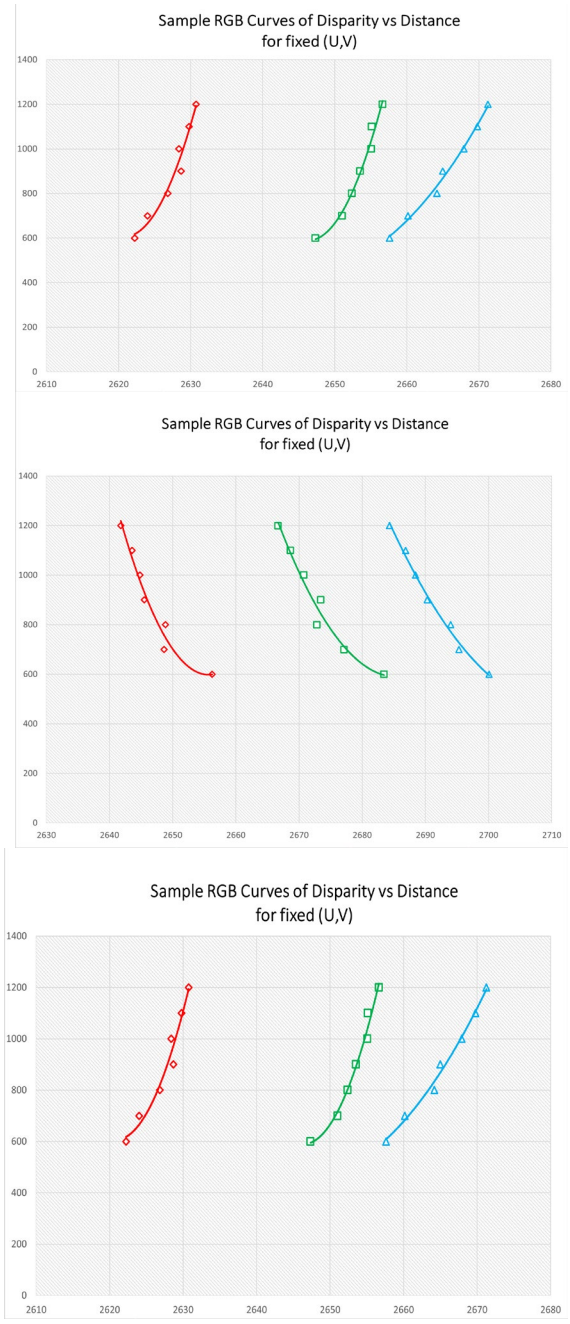

Figure 20 Sample disparity *vs* distance curves for fixed reference points in each row of targets. From top to bottom, the chosen targets were in the center, below the center and above it.

These curves show that the calibration points derived from individual targets, set at distances from 600 to 1200 mm, lay on smooth curves. To form the calibration look-up tables, the measured disparities from all the actual target points (~230 at different (u,v) image points in the

binocular region) were added to form sparse look-up tables. Although searching for the eight points neighboring any desired point to generate new distance maps may be formally computationally expensive, the small total size of the lookup tables makes using a more sophisticated and complex algorithm unjustified.

3.8 System costs

The system used a Raspberry Pi camera, costing roughly $US100 and a readily available right-angle prism costing less than $US 20. The RGB light sources used inexpensive strips of colored LEDs mounted on a white board, adding perhaps another $US 20.

4. Conclusion

A simple calibration technique for the flexible prism stereo system was described. Our system used readily available and inexpensive components - a small camera and a common 45° prism. A simply constructed circle target was used to generate calibration tables. The calibration system collects a set of images at known distances in the scene. Processing the images identified the circular targets used an OpenCV contour detector to locate the circle centers, matching corresponding points and building the sparse look-up tables.

4.1 Improving Accuracy

The partial curves in **Figure 19** show that the data from the three RGB channels show different disparity values, but similar patterns. This enables us to improve accuracy by using the monochrome sources to generate depth maps that can be averaged to improve accuracy. If unknown targets are imaged in three different bands, reflections from the monochrome sources will be, in the absence of fluorescence or phosphorescence contributions, themselves monochrome and not severely affected by the prism deviations: typical monochrome LEDs are quite narrow sources (usually 20-50 nm optical bandwidths) [22]. Thus, depth maps derived from each band can be reliably averaged to increase depth accuracy. This potential will be explored in a further paper.

4.2 Further improvements

After examining results from these trials, we noted that improvements might be made by:

1. using a larger number of smaller targets to increase the density of points in the calibration look-up tables: targets only need to be visible in the cameras and could be ~ 15 mm or even smaller, for high resolution cameras, than the 25 mm targets used here and
2. labelling more targets with, e.g. square, to speed up recognition of matching targets in the calibration stage.

4.3 Contributions

This work contributed the following:

1. a stereo system using a single camera built from inexpensive, readily available right-angle prisms, to generate 3D maps of a scene,
2. compared to previous work, custom low angle prisms were not required,
3. further, no mirrors, filters or expensive, e.g. telecentric, lenses were required,
4. simple optical arrangements without precise alignments were effective, compared to the complex hardware being used in other research, such as telecentric cameras, multiple mirrors, and beam splitters etc. [23].
5. readily available multicolor LED sources provided the monochromes sources and
6. the potential to improve accuracy by averaging results from the individual measurements at different optical bands requiring, at most, three image frames as the bands were switched.

The potential to use the simple optical requirements in underwater systems is also noted: the prism can be part of a sealed underwater housing.

References

[1] S. Hussmann, T. Ringbeck and B. Hagebeuker, "A Performance Review of 3D TOF Vision Systems in Comparison to Stereo Vision Systems," in *Stereo vision*, London, United Kingdom: IntechOpen Limited, 2008, ch. 7, pp. 103–120.

[2] J. -J. Aguilar, F. Torres and M. Lope, "Stereo vision for 3d measurement: accuracy analysis, calibration and industrial applications," *Measurement*, vol. 18, no. 4, pp. 193–200, 1996, doi: 10.1016/S0263-2241(96)00065-6.

[3] K. B. Lim, W. L. Kee and D. Wang, "Virtual camera calibration and stereo correspondence of single-lens bi-prism stereovision system using geometrical approach," *Signal Processing: Image Communication*, vol. 28, no. 9, pp. 1059–1071, 2013, doi: 10.1016/j.image.2013.08.002.

[4] M. Wang, "Theoretical and experimental study on a new reconstruction model based on geometric optics for a single-lens biprism-based stereovision system," *Measurement Science and Technology*, vol. 33, no. 8, 2022, Art. no. 085404, doi: 10.1088/1361-6501/ac6080.

[5] C. C. Slama, "Introduction," in *Manual of photogrammetry*, Falls Church, VA, USA: American Society of Photogrammetry, 1980, ch. 1, pp. 1–30.

[6] J. Heikkila and O. Silv´en, "A four-step camera calibration procedure with implicit image correction," in *Proc. IEEE computer society conference on computer vision and pattern recognition*, San Juan, PR, USA, 1997, pp. 1106–1112, doi: 10.1109/CVPR.1997.609468.

[7] Z. Zhang, "A flexible new technique for camera calibration," *IEEE Transactions on pattern analysis and machine intelligence*, vol. 22, no. 11, pp. 1330–1334, 2000, doi: 10.1109/34.888718.

[8] J. Zhang, H. Yu, H. Deng, Z. Chai, M. Ma and X. Zhong, "A robust and rapid camera calibration method by one captured image," *IEEE Transactions on Instrumentation and Measurement*, vol. 68, no. 10, pp. 4112–4121, 2019, doi: 10.1109/TIM.2018.2884583.

[9] R. Kala, "Perception in Autonomous Vehicles," in *On-road intelligent vehicles: Motion planning for intelligent transportation systems*, Cambridge, MA, USA: Butterworth-Heinemann, 2016, ch. 3, pp. 36–58.

[10] E. M. Mouaddib, R. Sagawa, T. Echigo and Y. Yagi, "Stereovision with a single camera and multiple mirrors," in *Proc. 2005 IEEE International Conference on Robotics and Automation*, Barcelona, Spain, 2005, pp. 800–805, doi: 10.1109/ROBOT.2005.1570215.

[11] K. Takahashi, S. Nobuhara and T. Matsuyama, "A new mirror-based extrinsic camera calibration using an orthogonality constraint," in *2012 IEEE Conference on Computer Vision and Pattern Recognition*, Providence, RI, USA, 2012, pp. 1051–1058, doi: 10.1109/CVPR.2012.6247783.

[12] J. Li, B. Zhang, X. Kang, W. Xu, G. Yang and L. Yang, "Single camera 3d digital image correlation using a polarized system," *Instruments and Experimental Techniques*, vol. 61, no. 1, pp. 99–105, 2018, doi: 10.1134/S0020441218010050.

[13] D. Lee and I. Kweon, "A novel stereo camera system by a biprism," *IEEE Transactions on Robotics and Automation*, vol. 16, no. 5, pp. 528–541, 2000, doi: 10.1109/70.880803.

[14] K. Genovese, L. Casaletto, J. A. Rayas, V. H. Flores and A. Martinez, "Stereo-digital image correlation (DIC) measurements with a single camera using a biprism," *Optics and Lasers in Engineering*, vol. 51, no. 3, pp. 278–285, 2013, doi: 10.1016/j.optlaseng.2012.10.001.

[15] B. Pan, D. Wu and Y. Xia, "An active imaging digital image correlation method for deformation measurement insensitive to ambient light," *Optics & Laser Technology*, vol. 44, no. 1, pp. 204–209, 2012, doi: 10.1016/j.optlastec.2011.06.019.

[16] B. Pan, L. Yu and Q. Zhang, "Review of single-camera stereo-digital image correlation techniques for full-field 3d shape and deformation measurement," *Science China Technological Sciences*, vol. 61, pp. 2–20, 2018, doi: 10.1007/s11431-017-9090-x.

[17] K. B. Lim and B. Qian, "Biprism distortion modeling and calibration for a single-lens stereovision system," *Journal of the Optical Society of America A*, vol. 33, no. 11, pp. 2213–2224, 2016, doi: 10.1364/JOSAA.33.002213.

[18] L. Yu and B. Pan, "Single-camera stereo-digital image correlation with a four-mirror adapter: optimized design and validation," *Optics and Lasers in Engineering*, vol. 87, pp. 120–128, 2016, doi: 10.1016/j.optlaseng.2016.03.014.

[19] L. Wu, J. Zhu and H. Xie, "Single-lens 3d digital image correlation system based on a bilateral telecentric lens and a bi-prism: validation and application," *Applied Optics*, vol. 54, no. 26, pp. 7842–7850, 2015, doi: 10.1364/AO.54.007842.

[20] Z. Hui, Z. Liyan, W. Hongtao and C. Jianfu, "Surface measurement based on instantaneous random illumination," *Chinese Journal of Aeronautics*, vol. 22, no. 3, pp. 316–324, 2009, doi: 10.1016/S1000-9361(08)60105-3.

[21] J. Morris and G. Gimel'farb, "High resolution stereo hardware implementation," US Patent US201100 91096A1, May, 4,2009.

[22] D. B. Murphy and M. W. Davidson, "Light and Color," in *Fundamentals of light microscopy and electronic imaging*, Hoboken, NJ, USA: John Wiley & Sons, 2012, ch. 2, pp. 21–32.

[23] K. Zhu and B. Pan, "Panoramic/dual-surface digital image correlation measurement using a single camera," *sensors*, vol. 22, no. 9, 2022, Art. no. 3266, doi: 10.3390/s22093266.